Where top-down meets bottom-up: Cell-type specific connectivity map of the whisker system

Rault N.[1], Bergmans T.[1], Delfstra N.[1], Kleijnen BJ[1], Zeldenrust F.[1] and Celikel T.[2]

[1]Donders Institute, Radboud University, Nijmegen, The Netherlands.
[2]Georgia Institute of Technology, Atlanta, GA, USA.

Abstract - Sensorimotor computation is a closed-loop process where bottom-up information collected about the current state of the world is integrated with top-down, internally generated knowledge, task- and goal-related affordances to create an action plan. In the rodent whisker system, a canonical model of sensorimotor computation in the context of active sensing, emerging evidence suggests that neuromodulatory neurotransmitters help shape sensorimotor control of the whisker position, and contribute to context-dependent changes in whisking frequency and amplitude. Given that neuromodulatory neurotransmitters are primarily released from subcortical nuclei whose long-range projections target the rest of the central nervous system, the circuit mapping of top-down neuromodulatory control of sensorimotor nuclei in the rodent brain will help to address the mechanisms of active sensing systematically. Therefore, taking advantage of the Allen Institute's Mouse Connectivity database, we provide an updated, cell-type specific map of the sensorimotor circuits in the mouse brain. The map includes 180 projections (65 of which were not previously reported in the literature) across 18 principal and neuromodulatory neurotransmitter-releasing nuclei of the whisker system. Performing a graph network analysis of this connectome, we identify cell-type specific hubs, sources, and sinks, provide anatomical evidence for monosynaptic inhibitory projections into all stages of the ascending pathway, and show that neuromodulatory projections improve network-wide connectivity. These results argue

that beyond the modulatory chemical contributions to information processing and transfer in the whisker system, the circuit connectivity features of the neuromodulatory networks position them as nodes of sensory and motor integration.

List of abbreviations

TG - Trigeminal Ganglion
PSV - Principal sensory nucleus
SPVO, SPVI, SPVC - spinal nucleus of the trigeminal oralis, interpolaris, caudalis
VPM - ventral posteromedial nucleus
PO - posterior complex of the thalamus
bfd - barrel field of the primary somatosensory cortex
MOp - primary motor cortex
SC - Superior Colliculus
VII - Facial Motor nucleus
ZI - Zona Incerta
SI - Substantia Innominata
DR - Dorsal raphe nucleus
LC - Locus coeruleus
PPN - Pedunculopontine nucleus
VTA - Ventral tegmental area
TM - Tuberomammillary nucleus

1 Introduction

In the wild, whisking rodents are subterranean mammals that live in dark and narrow environments. They heavily rely on the rhythmic protraction and retraction of their whiskers to navigate their natural habitat. Organized as closed-loop circuits (**Kleinfield et al., 1999**) distributed networks in the brain control whisking as an adaptive sensorimotor computation while they encode sensory information originating from the sensory periphery and compute the future position of the whiskers as an iterative process (**Voigt et al., 2008**, **Voigt et al., 2015**, **McElvain et al., 2018**).

The neural circuits that contribute to the sensory representations acquired through whisker contacts and the positional controls of whiskers were last summarized more than a decade ago **(Bosman et al., 2011)**. Building on the first comprehensive sensorimotor circuit map in the whisker system (**Kleinfield et al., 1999**) as well as the fundamental experimental work that described the lemniscal and paralemniscal ascending neural circuits (**Chial et al., 1991**, **Lu and Lin, 1992**), and the descending projections originating from the motor cortex (**Ashwell, 1982**, **Hemelt and Keller, 2008**), Bosman and colleagues described 74 connections across 12 nuclei in the whisker system and 6 brainstem regions that release neuromodulatory transmitters (**Supplemental Figure 1**).

Over the last decade, new experimental studies provided direct evidence that the network connectivity along the whisker system is more expansive than previously shown. For example, a study by **Minju Jeong et al., 2016**, focusing on the motor nuclei in the mouse, in particular MOp, revealed projections to PO and VPM in the thalamus, as well as to the contralateral PSV, SPV, and VTA. This latter connection and the monosynaptic MOp projections to PPN and SPVi were independently confirmed (**Rodrigo Muñoz-Castañeda et al., 2021**). In parallel, direct monosynaptic projections originating from bfd and targeting TM, RT, and ZI (**Izabela M. Zakiewicz et al., 2014**), ZI projections to VII (**Takatoh et al., 2021**), VII innervation of SPVi (**Bellavance et al., 2017**), VPM to MOp connections (**Bryan M. Hooks et al., 2013**) and bidirectional communication between MOp and RT were shown (**Yang et al., (2022)**).

The newly identified connections are not only among primarily sensory and motor nuclei. **Jonas A. Hosp et al., 2011** identified a projection between VTA and MOp, showing the contribution of dopaminergic connections originating from VTA in motor skill learning. Studies showed that VTA serves as a hub of divergence with projections to SI, LC, DR, RT (**Anna I. Dunigan et al., 2021**) and bfd (**Anna Aransay et al., 2015**), all critical for the information processing in the whisker system.

The novel discoveries along the neuromodulatory circuits and their integration with nuclei in the whisker system are not limited to the dopaminergic system. Monosynaptic cholinergic projections to RT (**Guela Sokhadze et al., 2018**), SI projections to ZI (**Zhou et al., 2018**), ZI projections to VTA (**An et al., (2021)**), reciprocal connections between PO and SC (**Benavidez et al., 2021**), SI projections to PSV, VTA, VPM, SI (**Benavidez et al., 2021**) and DR (**Benavidez et al., 2021**, **Dorocic et al., (2014)**) all provided anatomical evidence for neuromodulatory contributions to sensorimotor control.

These newly found connections require an update of the previously drawn connectivity map of the rodent whisker system. Here we provide the third-generation connectivity map using data publically made available by the Allen Brain Institute (**Oh, S.W. et al., 2014**) and an open-source toolbox we developed to systematically analyze the data (https://github.com/DepartmentofNeurophysiology/NeuralNet-ABC). By analyzing 211 anterograde tracing experiments performed in 53 wild-type and transgenic lines, we determine the connectivity along the ascending, descending, and neuromodulator pathways. We show that the sensorimotor circuits in the whisker system include 180 projections; 65 of these projections had not been described in the literature previously. By performing graph network analysis we further identify cell-type specific hubs, sources, and sinks in this connectome, and finally, show that neuromodulatory projections improve the network-wide connectivity.

2 Materials & Methods

2.1 Experimental pipeline

All experimental data is available online (https://connectivity.brain-map.org/) and experimental procedures have been detailed by the Allen Brain Institute before (**Oh, S.W. et al., 2014**). In short, genetically encoded fluorescent proteins were expressed in anatomically targeted regions using cell-type specific or non-specific promoters in transgenic and wild-type mice. The resulting anterograde projection labeling was visualized using serial two-photon tomography. The data were projected onto a normalized brain to identify anatomical origin and target areas based on a standard atlas (**Wang et al., 2020**). For each structure, four variables were extracted: the volume, the intensity, the density, and the energy. The volume represents the volume of tracer solution in mm^3 present in a brain structure; the intensity is the sum of the brightness of every pixel in a given structure (the tracer producing a fluorescent reaction); the density is the number of pixels considered as expressing the gene divided by the total amount of pixels present in the structure, and the energy is the sum of pixel intensities divided by the number of pixels in the structure. The results were stored in a JSON format containing the list of structures with their associated extracted variables. To build our connectivity matrices, we first downloaded the data using Allen Brain Institute's API (**Figure 1**), and identified experiments that targeted 18 target nuclei which have been experimentally identified as a part of the sensorimotor circuits in the rodent brain (**Supplemental Figure 1**). Each experiment was saved in a JSON file containing a list of structures (723 per hemisphere) and the measures of the projection volume, intensity, density, and energy. We then grouped the experiments per transgenic line and projected the data from each experiment onto a 723x1446 (723 structures for each hemisphere) with the sources of the experiments as rows and the structures receiving the connections as columns (**Figure 1**).

2.2 Transgenic categorization

Transgenic lines were considered "excitatory" if presented as such in the literature or if the marked cells were glutamatergic, i.e. for example, expressed glutamate or vesicular glutamate transporters and other proteins necessary for glutamatergic signaling. "Inhibitory" cells are classified as cells expressing Gamma-Aminobutyric Acid (GABA), glycine neurotransmitters, or other proteins related to inhibitory signaling, such as GABA receptors. Transgenic lines were classified as "uncategorized" if marked cells expressed both excitatory and inhibitory proteins, or if they expressed neither (e.g., dopamine, adrenaline, serotonin, or other neuromodulatory proteins with no direct excitatory or inhibitory effect). See **Supplemental Table 1** for the list and the corresponding citations.

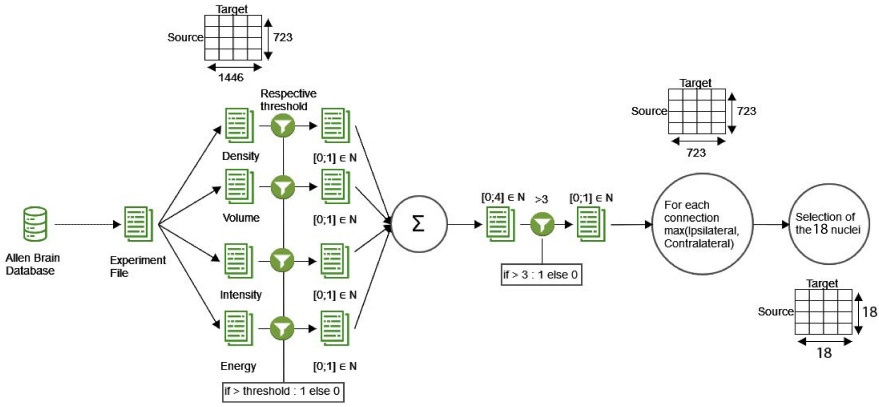

Fig. 1 The data processing pipeline. For each transgenic line, the data were downloaded from the Allen Brain database. Each experiment file was split into 4 matrices of size 723x1446, one per variable (density, volume, intensity and energy). A threshold specific to each variable (see Connectivity Validation) was applied and 4 matrices with values of either zero or one were retrieved. These matrices were summed and a threshold equal to 4 was applied, so that only the connections that satisfied the conditions on all 4 variables remained. This way, a matrix composed of zeros and ones was obtained. Due to the sparse nature of contralateral hemispheric projections, which will increase false negatives, the connectomes across the hemispheres were merged by selecting the highest value. From the resulting matrix of size 723x723, we retrieved the connections for the nuclei of interest (see Supplemental Figure 1.b and 1.c). This resulted in a binary connectivity matrix with 324 (18x18) possible edges.

2.3 Connectivity validation

To verify the validity of the connections appearing in the connectivity matrices built upon the Allen Brain Institute's experiments, we compared the identified connections to a subset (N=34) of connections reported by Bosman et al., 2011. For each variable, we obtained a variable-specific threshold by systematically increasing the threshold until 1 of the 34 reference connections was not found anymore in wild-type experiments. The last value for which we found 100% of true positives was taken as the correct threshold. Thus, we obtained four different thresholds that we applied on each transgenic line (density threshold: 0.0002416 (a.u.), intensity threshold: 110.8 (a.u.), energy threshold: 0.00668 (a.u.), volume threshold: 0.01559 (in mm^3)). To consider a connection as valid, we made sure that this connection appeared on each variable-specific matrix after threshold application. Consequently, we made sure to obtain previously found connections while not making any assumptions about the underlying connectivity, which would have happened if we relied on the more classical approach of trying to minimize the number of false positives. By relying only on true positives, we didn't assume any pattern of connectivity between the different nuclei. By cross-validating our connections with the four available variables we limited the possibilities of uncovering false negatives. As a final insurance, we made sure that the genes marked by the transgenic lines presented in the Allen Brain Institute's experiments were present in the targeted

structure with the transgenic characterization tool available on the Allen Brain Institute's website. After the application of these thresholds, we obtained four connectivity matrices, one for the wild type (**Figure 2.a and 2.b**) and one for each transgenic characterization (excitatory, inhibitory, or uncategorized, respectively: **Figure 3.a, 3.b and 3.c**). Calculations were repeated across animal lines to verify the connections (**Figure 4**). We finally built a summary map, containing previously observed and new connections. In this map, new connections were included only if they were validated by experiments on at least two different transgenic lines (**Figure 5.a and 5.b**).

2.4 Network analysis

From the obtained maps, we assessed the network properties of neuromodulator-releasing nuclei and their contribution to connectivity in the sensorimotor circuit. To determine the small-world nature of our network, we compared our summary graph with an Erdos-Renyi (ER) graph. We first determined the total number of connections in our summary map and computed the probability of a connection. We built an ER graph with the same number of edges, the same number of nodes, and the same probability of connection. We computed the clustering coefficient and the shortest path using the GRETNA toolbox (**Jinhui Wang et al., 2015**) for both the original and the ER graph. Watts and Strogatz defined a small-world network as presenting higher clustering values and a lower shortest path than ordered and random networks (**Watts and Strogatz, 1998**). We, therefore, considered our summary network to be a graph with small-world properties if its clustering coefficient was higher than the ER's clustering coefficient and its average shortest path was lower than the ER's average shortest path.

Next to the ER network, we built a summary graph without the neuromodulator releasing nuclei and computed the nodal clustering coefficient, the nodal shortest path, the degree centrality, the nodal efficiency, the nodal local efficiency, and the betweenness centrality. We then compared the distribution of these values to determine if the neuromodulator-releasing nuclei had an impact on the network structure.

3 Results

We extracted the data from 52 experiments on wild-type mice and 159 experiments on 52 different transgenic lines targeting the 18 nuclei (**Supplemental Figure 1**). Amongst the $18 \times 18 = 324$ possible connections for each type of mice, there were 237 connections in the wild-type strain. Experiments in the transgenic lines revealed 151 excitatory connections, 198 inhibitory connections, and 211 uncategorized connections presenting a value above 0 without threshold application. Of these 797 connections, 57.97% (i.e. 462 projections) met the criteria for anatomical connections (see Materials and Methods). For the considered structures, **Bosman et al., 2011** observed 74 connections (**Supplemental Figure 1.b, 1.c**), our study shows 161 connections for the

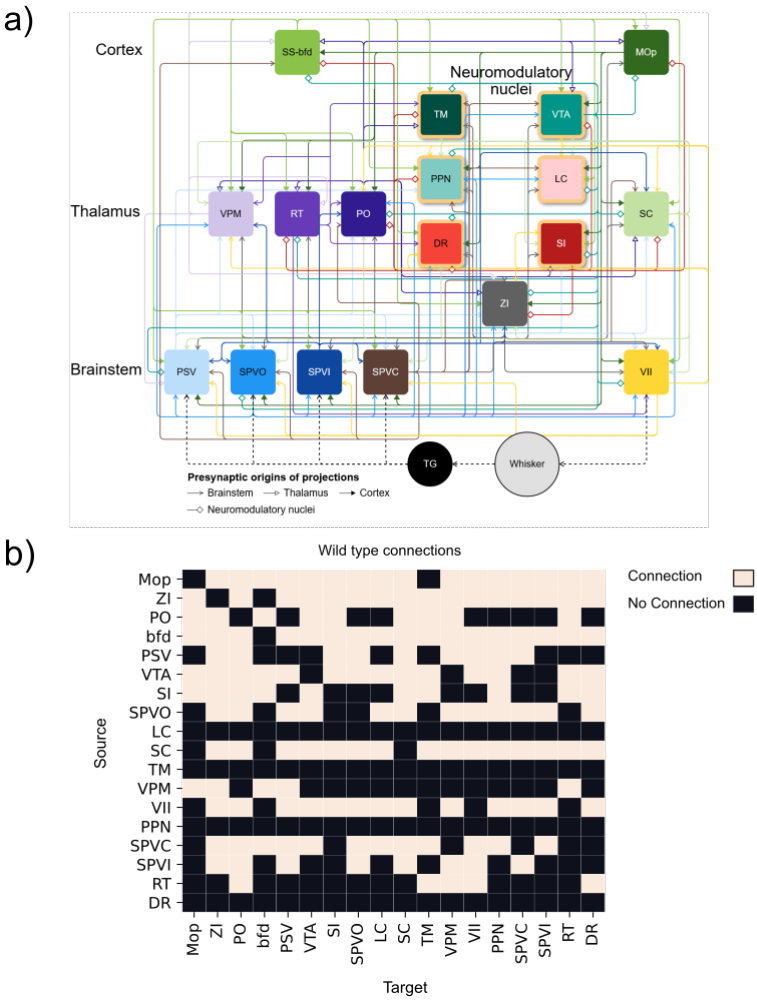

Fig. 2 The sensorimotor connectivity map of the whisker system in wild-type mice. **a)** The connectivity map across 18 nuclei with 161 connections was computed from wild-type experiments in the Allen Brain database. **b**) A binary representation of the connectivity matrix. LC, TM, PPN, and DR were not targeted in wild-type animals, thus their projections to the rest of the network are not shown. See Figure 3 for the results from transgenic animals and Figure 6 for the compiled connectome.

wild type (**Figure 2.a, 2.b**) and 301 connections for the 49 transgenic lines investigated on these structures and showing connections, distributed amongst the different connectivity maps. Amongst those connections, 73 are excitatory connections (**Figure 3.a**; **Supplemental Figure 2**), 104 are inhibitory connections (**Figure 3.b**; **Figure 4**) and 124 are uncategorized connections (**Figure 3.c**; **Supplemental Figure 3**), amongst which 32 don't appear on excitatory or inhibitory connectivity maps (**Figure 3.d**). There is an overlap of 22% between excitatory connections and inhibitory connections, 30%

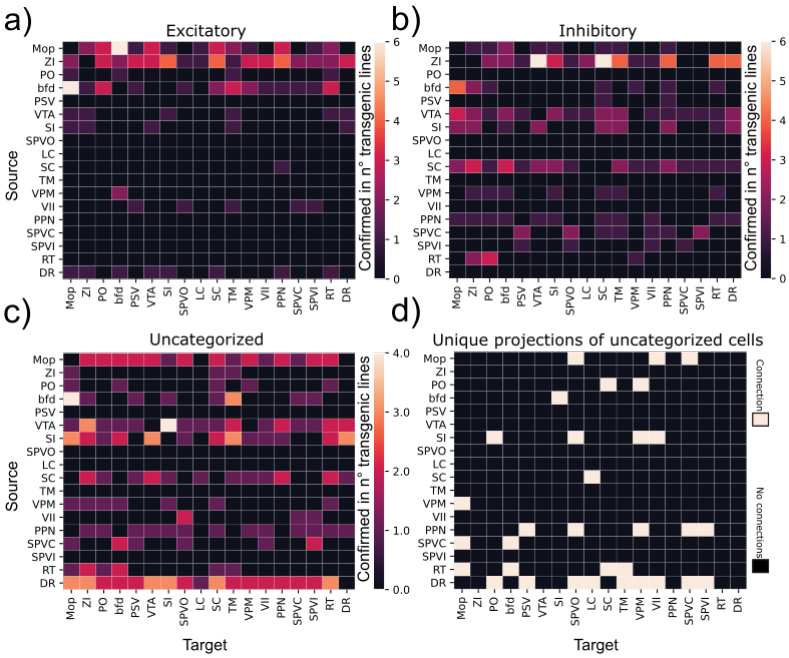

Fig. 3 Cell type specific sensorimotor connectomes. The vertical axes represent the source, and the horizontal ones are the target. In a-c, the colors represent the number of transgenic lines confirming the connection. **a)** Experiments on excitatory transgenic lines unveiled 73 connections, mostly originating from the cortex and the zona incerta. **b)** A total of 104 connections were discovered in inhibitory transgenic lines. **c)** Experiments on uncategorized transgenic lines unveiled 124 connections. Note the divergence of projections originating from VTA, SI, PPN, and DR, all neuromodulatory neurotransmitter-releasing nuclei. **d)** A binary representation of unique projections in cell classes that either express both excitatory and inhibitory marker or neither. A total of 32 connections were identified, none of which appeared in excitatory or inhibitory connectomes of the sensorimotor circuit.

between inhibitory connections and uncategorized connections, and finally 22% between excitatory connections and uncategorized connections.

Amongst the structures presented in this study, the tuberomammillary nucleus, the locus coeruleus and the oral part of the spinal nucleus have not been targeted by experiments in the Allen Brain database. Also, on the wild-type map, the Tuberomammillary nucleus, the Pedunculopontine nucleus, the Locus coeruleus, and the Dorsal nucleus raphe have not been covered in the Allen Brain database.

In the next sections, we will discuss the connections originating from each nucleus, validated by our methods.

3.1 Trigeminal nuclei

The information originating upon whisker contact with a surface propagates along brainstem, thalamus, and primary somatosensory cortex while making close-loop connections with the motor system (**Kleinfeld et al., 1999**). The

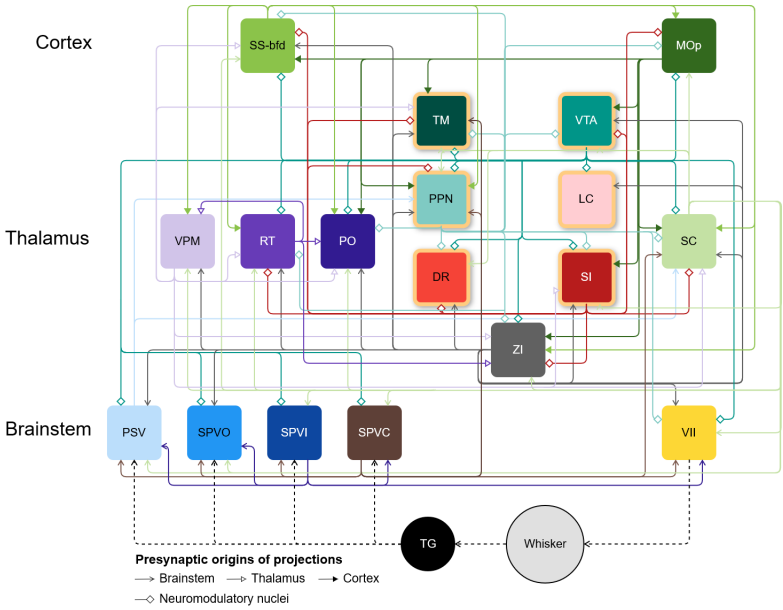

Fig. 4 The connectome of the inhibitory projections in the mouse whisker system. The connectivity map includes 104 connections.

contact-induced information is not only excitatory as inhibition is recorded early in the sensory axis (**Kleinfeld et al., 1999**). Therefore, maybe not surprisingly, we found that PSV, SPVi, and SPVc contain inhibitory presynaptic cells that suggest inhibitory and excitatory activity contribute to information processing of the sense of touch as early as in the brainstem (**Figure 5**).

Additionally, the ascending pathway, traditionally described as being trisynaptic, appears incomplete as monosynaptic connections between the brainstem and bfd were uncovered in our study.

We identified 2 inhibitory connections originating from PSV targeting SC and PPN. Connections to VPM, PO, SI, ZI, SPVO, SPVC, and VII were identified but the cell type specificity of the origins of these connections is not clear at this time. The connections to SPVO and SPVC were present in wild-type as well as transgenic experiments, while they were not observed in any previous studies.

Inhibitory origin of the presynaptic projections from SPVi to trigeminal nuclei and VII argue inhibitory control of touch processing at the brainstem level. In addition, uncategorized connections were found to target VPM, PO, ZI, and SC. The connections targeting SPVo and SPVc were validated by transgenic and wild-type experiments, while not observed in any previous studies.

SPVc inhibits the trigeminal nuclei, PPN, SC, and VII. Uncategorized connections were found targeting bfd, PO, TM, VTA, LC, and ZI. The connections toward bfd and SPVo were validated by transgenic and wild-type

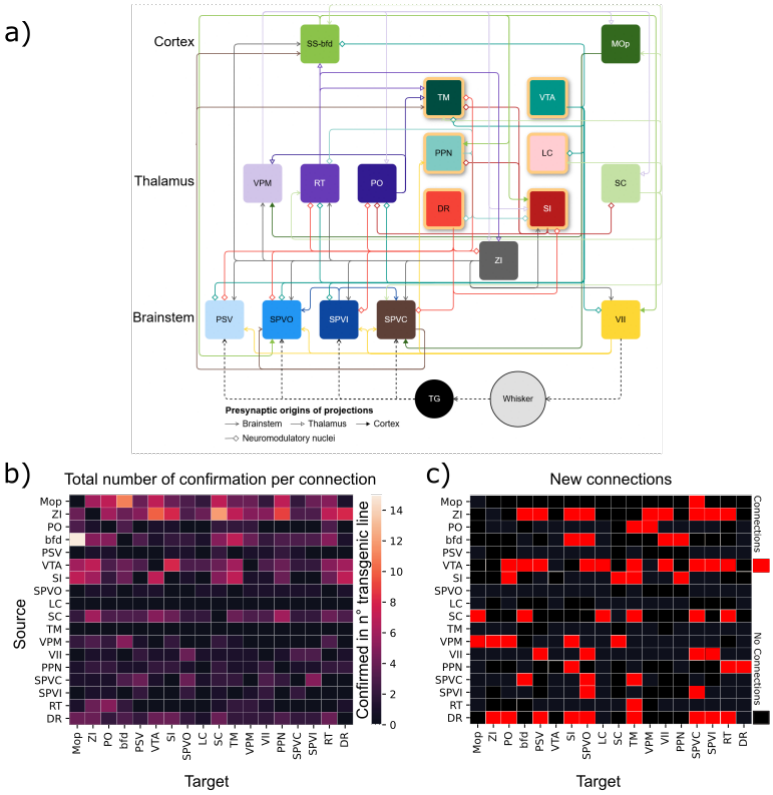

Fig. 5 Newly discovered monosynaptic projections across the sensorimotor map of the mouse whisker system. a) A graphical representation of the connectome. **b)** 213 connections were identified in the experiments from the Allen Brain database. 180 of these connections were confirmed in at least two mouse lines and have been included in the final connectome (Figure 6). The vertical axis represents the source of the connection, and the horizontal axis the target. The color scale indicates the number of mouse lines that confirm the presence of the connections. **c)** 65 out of 180 projections have not been previously described in the literature to the best of our knowledge.

experiments and were not observed in any previous studies. These findings support previous observations (**Jacquin et al., 1990**) which demonstrated dense intersubnuclear connections in the trigeminal complex of the rat. We build on these observations and demonstrate that inhibitory presynaptic cells in the trigeminal complex target the other trigeminal nuclei and provide long-range connections to low-level structures from the motor pathway and acetylcholine-releasing nucleus. As described in **Esmaeili et al., 2020**, acetylcholine is believed to play a role in associating a whisker stimulus with a reward expectation. Through a direct connection from the trigeminal nuclei to PPN, low-level structure of the ascending somatosensory pathways can modulate cholinergic reward signals.

3.2 Thalamus

Traditionally thalamic nuclei of the somatosensory system are considered as relay nuclei that contribute to the spatiotemporal representation of touch (**Ahissar and Arieli, 2001, Azarfar et al., 2018**). Feed-forward excitatory projections originating from VPM and PoM and targeting the barrel field cortical columns and septa, respectively, are believed to be the primary pathway of information flow (**Kleinfield et al., 1999**). Our anatomical study has surprisingly shown that these projections also include feed-forward inhibition as well as forming intrathalamic inhibitory communication between VPM and PoM.

Inhibitory and excitatory cells were found to be the origins of long-range connections originating from VPM. Direct excitation by VPM of bfd was found as well as direct inhibition (**Supplemental Figure 4**) of bfd, SC, ZI, RT, and PO by this nucleus. Uncategorized connections were found to target MOp and PSV. The connection originating from VPM and targeting ZI was found in transgenic and wild-type experiments, while not observed in any previous studies. PO was found to excite RT, TM, bfd, and MOp. Uncategorized connections toward VPM, ZI, SI, VTA, and SC were found. Connections targeting SC, VPM, and TM as shown in transgenic and wild-type experiments were not observed before.

Inhibitory connections originating from RT target VPM, PO, and ZI. VII and TM are targeted by a connection with unclear presynaptic cell types in RT. The connection toward TM has been validated in transgenic and wild-type experiments but was not observed earlier in the literature.

While inhibition of the somatosensory thalamus is believed to be mainly the result of ZI and RT activity (**Barthó et al., 2002**) we demonstrated the presence of presynaptic inhibitory neurons in VPM, connecting, in particular to PO. Whether these projections could mediate the inhibition of the paralemniscal pathway by the lemniscal pathway will need to be tested physiologically.

3.3 Barrel field of the primary somatosensory cortex

The information flow that translates whisker sensation to whisker movement is commonly seen as a bottom-up integration followed by a top-down propagation of neural activity resulting in the activation of the facial muscles. However, our study has shown top-down regulation of sensory information from bfd to the brainstem and the thalamus through monosynaptic excitation.

Bfd sends long-range connections to low-level structures in the whisker system. The barrel field excites the trigeminal nuclei, the three nuclei of the thalamus that we considered, TM, MOp, SC, and VII and inhibit RT, MOp, SC, and ZI. Connections were found toward VTA, LC, SI, PPN, and DR, however, they remain uncategorized at this time. New direct connections to SPVC, SPVI, SPVO, VTA, and VII were identified in transgenic and wild-type experiments. Top-down excitation of the trigeminal nucleus and facial motor

nucleus by bfd was found in our study as well as a monosynaptic connection to dopaminergic nucleus (VTA). This later connection shows that bfd can have a direct influence on dopamine release, allowing the primary somatosensory cortex to impact the circuit described in **Esmaeili et al., 2020**, linking whisker sensation to reward outcome.

3.4 Primary Motor cortex

Excitatory connections were found to target bfd, PO, PPN, VTA, SC, Dr, and ZI from MOp. MOp also inhibits the same structures with the exception of DR and the addition of TM and SI. Uncategorized connections were found targeting LC, RT, VPM, VII, and the trigeminal nuclei. All of the connections appearing in transgenic and wild-type experiments have been described in the literature previously.

3.5 Superior Colliculus

In the map previously described by **Bosman et al., 2011** the superior colliculus contribution to sensorimotor integration was limited to connections to ZI, PPN, and VII. Our study revealed that SC was the most connected node in this network. Additionally, SC appears to be mainly the origin of inhibitory connections spanning across the entire sensorimotor and neuromodulatory system.

Excitatory and inhibitory connections were found to originate from SC. Excitatory SC projections target PPN while inhibitory projections monosynaptically activate targets in TM, PPN, VTA, MOp, SI, ZI, the thalamus, PSV, and VII. Connections toward LC, SPVo, SPVi, and SPVC were identified but remain uncategorized at this time. New connections toward TM, SI, and RT were found in transgenic and wild-type experiments. ZI and RT being known to inhibit the activity of the somatosensory thalamus (**Nicolelis et al., 1990**, **Lam and Sherman, 2007**) were found to be inhibited by SC which could therefore be a source of disinhibition in the whisker system of the rodent.

3.6 Facial motor nucleus

The facial motor nucleus, composed of premotoneurons, is the last nucleus of the descending motor pathway sending commands to the periphery to produce whisker movement (**Ashwell, 1982**). In this study, we found connections originating from VII targeting various nuclei in the whisker system. In particular, connections targeting the trigeminal nuclei were identified. These structures, being the first nuclei to integrate whisker information in the brain, are also targeting VII (see Trigeminal nuclei section). The interplay between VII and the trigeminal nuclei might be a part of a low-level loop integrating sensory information and producing whisker movement without requiring activity from higher structures. The facial motor nucleus was found to excite TM and the trigeminal nuclei. Uncategorized connections were found to target VPM, PO, DR, ZI, SI SC, LC, and VTA. The connections toward PPN, PSV, and SPVO

were identified in transgenic and wild-type experiments and had not been observed before. Reciprocal connections between the trigeminal nuclei and VII should be further investigated to understand the role of low-level loops in the whisker system of the rodent.

3.7 Zona Incerta

The zona incerta is classically described as one of the main inhibition sources in the rodent's whisker system (**Venkataraman et al., 2021**). Our study revealed that ZI could also send excitatory monosynaptic projections to every nucleus analyzed in our study. In addition, inhibitory connections were found to target the thalamic nuclei, PSV, DR, PPN, TM, bfd, VII, SI, SC, LC, and VTA. New connections targeting VII, DR, VPM, PSV, SPVI, and SPVC were identified in transgenic and wild-type experiments. While most studies targeting ZI report GABAergic connections (**Ficalora and Mize, 1989**, **Nicolelis et al., 1992**, **Nicolelis et al., 1990**) existence of the excitatory projections that target the entire sensorimotor network described herein suggest that ZI, along with SC, serves as primary nodes of divergence in this network.

3.8 Neuromodulatory projections

VTA has a role in learning the association of a whisker stimulus to a potential reward (**Esmaeili et al., 2020**). Our results revealed that VTA's contribution to the whisker system function is not necessarily mediated by dopaminergic connections; excitatory and inhibitory presynaptic neurons in VTA target other nuclei. VTA sends excitatory connections to bfd, RT, TM, MOp, SI, DR, and ZI and inhibitory projections to every nucleus of the subnetwork except VPM. New connections toward bfd, TM, LC, VII, DR, PO, RT, SPVO, and PSV were found in transgenic and wild-type experiments.

Cholinergic connections have also been hypothesized to play a role in transforming whisker sensation into a licking action (**Esmaeili et al., 2020**). Consequently, it is not surprising to see connections originating from SI targeting bfd and MOp. However, as for VTA, we witnessed a large number of connections, mainly inhibitory, targeting the other neuromodulator-releasing nuclei. This shows that SI has the ability to regulate the activity of other nuclei form the neuromodulatory system. In particular, SI inhibits PPN, another nucleus from which cholinergic connections can originate. SI sends excitatory connections to DR, TM, ZI, and MOp and inhibitory connections to RT, bfd, TM, PPN, DR, ZI, SC, and VTA. One connection with non-specific presynaptic cells was unveiled toward PO. New connections to SC, VTA, TM, PPN, DR, PO, and RT were found in transgenic and wild-type experiments.

Excitatory connections from DR were found to target RT, ZI, SI, PPN, SC, VTA, MOp, and bfd. Since no wild-type experiments were conducted on DR, none of the aforementioned connections could be validated as new connections, i.e not previously described in the literature.

3.9 Network analysis

In order to measure the contribution of neuromodulator-releasing nuclei to the network, we compared the path length and clustering coefficient between the summary graph and the ER graph (see Materials and Methods). This analysis revealed no difference in structure between the sensorimotor pathway and the ER graph in terms of clustering coefficient (mean ER = 0.66 ±0.02 std, mean summary graph = 0.68±0.14 std, p-value = 0.6884) and shortest path (mean ER = 1.21 ±0.11 std, mean summary graph = 1.23 ±0.08 std, p-value=0.0677). Thus, we conclude that the found network doesn't present small-world properties.

Our comparison between the network with neuromodulator-releasing nuclei and without these revealed no differences in terms of nodal clustering coefficient (mean neuromod = 0.64 ±0.11 std, mean no-neuromod = 0.68 ±0.14 std, p-value=0.7694), nodal efficiency (mean neuromod = 0.81 ±0.06 std, mean no-neuromod = 0.82 ±0.06 std, p-value=0.5121), nodal local efficiency (mean neuromod = 0.78 ±0.11 std, mean no-neuromod = 0.79 ±0.13 std, p-value=0.6063), nodal shortest path (mean neuromod = 1.24 ±0.10 std, mean no-neuromod = 1.23 ±0.08 std, p-value=0.4632), efficiency (mean neuromod = 0.35 ±0.05 std, mean no-neuromod = 0.36 ±0.06 std, kl-divergence = 0.01) and clustering (mean neuromod = 0.29 ±0.05 std, mean no-neuromod = 0.31 ±0.06 std, p-value=0.7696). The degree centrality, on the other hand, was significantly higher when neuromodulatory nodes were included the connectome (mean neuromod = 10.75 ±2.01 std, mean no-neuromod = 7 ±1.15 std, p-value=0.0001), so was the betweenness centrality (mean neuromod = 4.67 ±4.7 std, mean no-neuromod = 2.08 ±1.74 std, p-value=0.0456). These results suggest that the neuromodulator nodes in the nodes of convergence/divergence in this sensorimotor network.

Next, we aimed to identify hubs in the network. Therefore, we focused on the role of each nucleus in the excitatory, inhibitory, and summary graphs, to identify the presence of hubs.

The average amount of connections sent (divergence) by a node was greater than the average amount of connections received (convergence) by a node in the inhibitory network (mean # input connections = 5.11 ±2.10 std, mean # output connections = 7.66 ±4.26 std), in the excitatory network (mean # input connections = 3.66 ±1.37 std, mean # output connections = 6.6 ±4.52 std) and in the wild type network (mean # input connections = 8.94 ±1.71 std, mean # output connections = 11.5 ±3.81 std). Amongst the nodes in the excitatory network, we identified that ZI was sending connections to more than 90% of the network. MOp and bfd connect to more than 70% of the nodes. We, therefore, considered these three nuclei to be source hubs in the excitatory graph.

In the inhibitory graph, VTA and SC sent connections to more than 80% of the nodes and ZI connects to more than 70% of them. VTA, SC, and ZI are therefore considered source hubs in this network

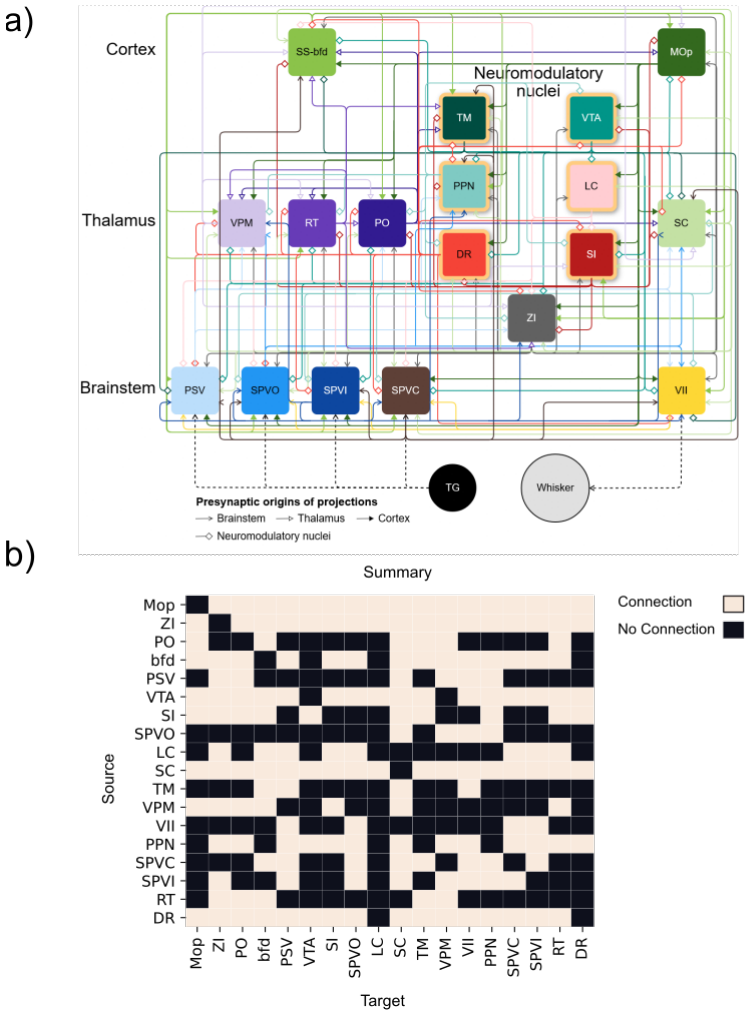

Fig. 6 The sensorimotor connectivity map of the mouse whisker system. Data from all animal lines are combined. **a)** A total of 180 connections were found and confirmed either by previous work or by at least two different types of mice. **b)** A binary connectivity matrix that summarizes pairwise connectivity in the network.

MOp, ZI, and SC are connected to more than 90% of all nodes, VTA and DR more than 80% whereas bfd and PPN connect to more than 70% of the graph. These nuclei are therefore considered source hubs in our network. Only SC receives connections from more than 70% of the nodes making it the only possible sink hub in it.

4 Discussion

We presented an extensive connectome of the whisker system of the mouse (**Figure 5**) and identified the cell-type-specific hubs, sinks, and sources in the connectome.

The network has a total of 180 connections, which represent 55.56% of all possible connections in our subnetwork with 18 nodes. 65 of these connections have not been described in the literature to the best of our knowledge. Given the fact that the 18 nuclei are selected based on their experimentally confirmed contribution to sensorimotor integration, this high connectivity seems plausible. To ensure that the data is not biased due to false positives/negatives, we repeated the analysis in different lines of animals (**Figure 4**). Our summary map (**Figure 5**) only those connections were confirmed by at least two lines.

While the considered structures have a role in sensorimotor integration, it is likely that some revealed connections don't contribute directly to sensorimotor processing. It is also important to note that some structures (**Supplementary Material - Table 2**), such as the neuromodulator releasing nuclei, were targeted by only a few if any, experiments. These connections have to be further investigated.

Our network analysis revealed that the neuromodulator-releasing nuclei, while not being the most targeted structures by experiments (**Supplementary Material - Table 2** - LC, TM, PPN), project to other targets in every stage of sensorimotor integration. These nuclei present a higher out-degree than in-degree. In fact, the amount of incoming connections throughout the network only slightly varies between nuclei. This demonstrates that the nuclei of this system are highly interconnected. Revealing the networks of information flow will require targeted distributed recordings across the sensorimotor connectome.

VTA and DR send connections to more than 80% of the nuclei and PPN targets more than 70% of them. Despite the identification of the contribution of several of these connections, a significant portion still remains unexplained. VTA, SI, and DR present a large amount of unclear outgoing connections, which have to be further investigated since each of these connections can be respectively a dopaminergic, a cholinergic, or a serotonergic connection.

While the results of our network analysis didn't show small-world properties, we need to keep in mind that we preselected a highly interconnected network in which every nucleus has a role to play. These results show that even though some nuclei could be "cut" from the network, the information could still flow, which argues for the robustness of the network organization. On the other hand, degree centrality and the betweenness centrality analysis showed that the neuromodulator-releasing nuclei are highly interconnected in the network since their absence totally shifts the distribution of these coefficients.

The identification of connection types informs us about the structure of the network. Identifying the time sequence in which the nuclei are solicited upon external stimulus presentation would require a functional analysis of this network. By relying on identified transgenic lines, our study allowed us

to determine the interactions between the nuclei as well as the central role of ZI, which demonstrated a high degree of connectivity of both excitatory and inhibitory nature. The available data also showed that VII's contribution is mainly of excitatory nature, with a systematic excitation of the trigeminal nuclei, while almost all connections originating from SC are inhibitory. SPVC and SPVI appear to inhibit all other trigeminal nuclei. As discussed in **Furuta et. al, 2008**, it is unlikely that such a connection would appear to originate from SPVO. Ppp1r17-Cre-NL1 inhibitory neurons originating from VPM and targeting PO were also unveiled. Overall, our results unveiled more inhibitory connections than excitatory or uncategorized ones, showing that inhibition happens at every stage of sensorimotor integration. Interestingly, we demonstrated inhibition at low-level structures of the brain, in particular the trigeminal nuclei and the thalamus. As inhibition makes it more difficult for information to travel from one nucleus to the other, this suggests computational complexity already at early stages of sensory processing. In the brainstem, while inhibition was already known to occur in the barrelettes local circuit (**Lo et al., 1999**) and by SPVI and SPVC or PSV, no previous studies attested the presence of inhibition between the different spinal nuclei. A functional study should be performed and the resolution should be increased in order to understand the source and the role of these connections. Inhibition from PSV also targets SC, VII, and PPN, hinting at a possible direct role of sensory input in inhibiting motor activity generated by low-level structures, and in regulating acetylcholine release in the system. The source of inhibition in VPM also points to the fact that RT is not the only source of inhibition in the thalamus and that the gating of whisker information might occur based on VPM's activity. It is also important to note the lack of ascending excitatory connections between the trigeminal nuclei and the thalamus. Because of the low amount of transgenic lines investigated on these structures, the lines responsible for these connections likely remain uncovered.

While the intertwining of the motor pathways and the sensory pathways is known in the cortex, our results point out that such interlinking occurs at every stage of the sensorimotor pathway, with SC being the most connected nucleus in the network and VII receiving 11 connections out of 17 possible ones (recurrent connections not considered). This leads us to think that motor control doesn't necessarily require the solicitation of MOp to actuate the whiskers. The multiple connections originating from earlier stages of the somatosensory pathway might be sufficient to regulate movements based on sensory stimuli, while the connections from the motor pathway might offer many possibilities for efferent copies to occur, as no proprioceptors reside in the whisker follicles (**Kyle S. Severson et al., 2019**).

In this study, we used the Allen Brain database to unveil 65 new connections and to categorize their nature, improving the granularity of our understanding of the subnetwork's connectome and showing that inhibition occurs at every stage of information processing. We pointed out the role of low-level structures as well as the neuromodulator releasing nuclei thanks to graph analysis. While

we drew a clearer picture of how the sensorimotor pathway integrates whisker information, it is necessary to couple these results to functional studies and increase the number of transgenic lines tested on this subnetwork, to determine the role of each connection related to sensorimotor integration. While we improved the previous connectivity map, grasping a full understanding of the sensorimotor pathway in the whisker system of the rodent still requires more work. In particular, tracing experiments with higher granularity or on low-level structures and neuromodulator-releasing nuclei, as well as functional studies need to be performed. Only by a combination of these can one then be able to propose a biologically inspired computational model of the whole network.

Acknowledgment

This project has received funding from the European Union's Horizon 2020 research and innovation program under the Marie Skłodowska-Curie grant agreement No 860949.

References

[1] Ahissar, E., & Arieli, A. (2001). Figuring Space by Time. Neuron, 32(2), 185–201. https://doi.org/10.1016/s0896-6273(01)00466-4

[2] An, S., Li, X., Deng, L., Zhao, P., Ding, Z., Han, Y., ... & Gong, H. (2021). A whole-brain connectivity map of VTA and SNc glutamatergic and GABAergic neurons in mice. Frontiers in Neuroanatomy, 15, 818242.

[3] Aransay, A. M., Rodríguez-López, C., García-Amado, M. A., Clascá, F., & Prensa, L. (2015). Long-range projection neurons of the mouse ventral tegmental area: a single-cell axon tracing analysis. Frontiers in Neuroanatomy, 9. https://doi.org/10.3389/fnana.2015.00059

[4] Ashwell KW. The adult mouse facial nerve nucleus: morphology and musculotopic organization. J Anat. 1982 Oct;135(Pt 3):531-8. PMID: 7153172; PMCID: PMC1169402.

[5] Azarfar, A., Calcini, N., Huang, C., Zeldenrust, F., & Celikel, T. (2018). Neural coding: A single neuron's perspective. Neuroscience & Biobehavioral Reviews, 94, 238-247.

[6] Bartho, P., Freund, T. F., & Acsády, L. (2002). Selective GABAergic innervation of thalamic nuclei from zona incerta. European Journal of Neuroscience, 16(6), 999-1014.

[7] Bellavance, M. A., Takatoh, J., Lu, J., Demers, M., Kleinfeld, D., Wang, F., & Deschênes, M. (2017). Parallel inhibitory and excitatory trigemino-facial feedback circuitry for reflexive vibrissa movement. Neuron, 95(3), 673-682.

[8] Benavidez, N. L., Bienkowski, M. S., Zhu, M., Garcia, L. H., Fayzullina, M., Gao, L., ... & Dong, H. W. (2021). Organization of the inputs and outputs of the mouse superior colliculus. Nature communications, 12(1), 4004.

[9] Bosman, L. W. J., Houweling, A. R., Owens, C. B., Tanke, N., Shevchouk, O. T., Rahmati, N., Teunissen, W. H. T., Ju, C., Gong, W., Koekkoek, S. K. E., & de Zeeuw, C. I. (2011). Anatomical Pathways Involved in Generating and Sensing Rhythmic Whisker Movements. Frontiers in Integrative Neuroscience, 5. https://doi.org/10.3389/fnint.2011.00053

[10] Cheng L, Arata A, Mizuguchi R, Qian Y, Karunaratne A, Gray PA, Arata S, Shirasawa S, Bouchard M, Luo P, Chen CL, Busslinger M, Goulding M, Onimaru H, Ma Q. Tlx3 and Tlx1 are post-mitotic selector genes determining glutamatergic over GABAergic cell fates. Nat Neurosci. 2004 May;7(5):510-7. doi: 10.1038/nn1221. Epub 2004 Apr 4. PMID: 15064766.

[11] Chiaia, N.L., Rhoades, R.W., Bennett-Clarke, C.A., Fish, S.E. and Killackey, H.P. (1991), Thalamic processing of vibrissal information in the rat. I. Afferent input to the medial ventral posterior and posterior nuclei. J. Comp. Neurol., 314: 201-216. https://doi.org/10.1002/cne.903140202

[12] Daigle TL, Madisen L, Hage TA, Valley MT, Knoblich U, Larsen RS, Takeno MM, Huang L, Gu H, Larsen R, Mills M, Bosma-Moody A, Siverts LA, Walker M, Graybuck LT, Yao Z, Fong O, Nguyen TN, Garren E, Lenz GH, Chavarha M, Pendergraft J, Harrington J, Hirokawa KE, Harris JA, Nicovich PR, McGraw MJ, Ollerenshaw DR, Smith KA, Baker CA, Ting JT, Sunkin SM, Lecoq J, Lin MZ, Boyden ES, Murphy GJ, da Costa NM, Waters J, Li L, Tasic B, Zeng H. A Suite of Transgenic Driver and Reporter Mouse Lines with Enhanced Brain-Cell-Type Targeting and Functionality. Cell. 2018 Jul 12;174(2):465-480.e22. doi: 10.1016/j.cell.2018.06.035. PMID: 30007418; PMCID: PMC6086366.

[13] Daigle, T. L., Madisen, L., Hage, T. A., Valley, M. T., Knoblich, U., Larsen, R. S., ... & Zeng, H. (2018). A suite of transgenic driver and reporter mouse lines with enhanced brain-cell-type targeting and functionality. Cell, 174(2), 465-480.

[14] Dorocic, I. P., Fürth, D., Xuan, Y., Johansson, Y., Pozzi, L., Silberberg, G., ... & Meletis, K. (2014). A whole-brain atlas of inputs to serotonergic neurons of the dorsal and median raphe nuclei. Neuron, 83(3), 663-678.

[15] Dunigan, A. I., Swanson, A. G., Olson, D. L., & Roseberry, A. G. (2021). Whole-brain efferent and afferent connectivity of mouse ventral tegmental area melanocortin-3 receptor neurons. Journal of Comparative Neurology, 529(6), 1157–1183. https://doi.org/10.1002/cne.25013

[16] Esmaeili, V., Tamura, K., Foustoukos, G., Oryshchuk, A., Crochet, S., & Petersen, C. C. (2020). Cortical circuits for transforming whisker sensation into goal-directed licking. Current Opinion in Neurobiology, 65, 38-48.

[17] Ficalora, A. S., & Mize, R. R. (1989). The neurons of the substantia nigra and zona incerta which project to the cat superior colliculus are GABA immunoreactive: a double-label study using GABA immunocytochemistry and lectin retrograde transport. Neuroscience, 29(3), 567-581.

[18] Furuta, T., Timofeeva, E., Nakamura, K., Okamoto-Furuta, K., Togo, M., Kaneko, T., & Deschenes, M. (2008). Inhibitory Gating of Vibrissal Inputs in the Brainstem. Journal of Neuroscience, 28(8), 1789–1797. https://doi.org/10.1523/jneurosci.4627-07.2008

[19] Harris JA, Hirokawa KE, Sorensen SA, Gu H, Mills M, Ng LL, Bohn P, Mortrud M, Ouellette B, Kidney J, Smith KA, Dang C, Sunkin S, Bernard A, Oh SW, Madisen L, Zeng H. Anatomical characterization of Cre driver mice for neural circuit mapping and manipulation. Front Neural Circuits. 2014 Jul 10;8:76. doi: 10.3389/fncir.2014.00076. PMID: 25071457; PMCID: PMC4091307.

[20] Hattox, A., Li, Y., & Keller, A. (2003). Serotonin Regulates Rhythmic Whisking. Neuron, 39(2), 343–352. https://doi.org/10.1016/s0896-6273(03)00391-x

[21] Hemelt, M. E., & Keller, A. (2008). Superior Colliculus Control of Vibrissa Movements. Journal of Neurophysiology, 100(3), 1245–1254. https://doi.org/10.1152/jn.90478.2008

[22] Hooks, B. M., Mao, T., Gutnisky, D. A., Yamawaki, N., Svoboda, K., & Shepherd, G. M. (2013). Organization of cortical and thalamic input to pyramidal neurons in mouse motor cortex. Journal of Neuroscience, 33(2), 748-760.

[23] Hosp, J. A., Pekanovic, A., Rioult-Pedotti, M. S., & Luft, A. R. (2011). Dopaminergic Projections from Midbrain to Primary Motor Cortex Mediate Motor Skill Learning. The Journal of Neuroscience, 31(7), 2481–2487. https://doi.org/10.1523/jneurosci.5411-10.2011

[24] Isa, T., Marquez-Legorreta, E., Grillner, S., & Scott, E. K. (2021). The tectum/superior colliculus as the vertebrate solution for spatial sensory integration and action. Current Biology, 31(11), R741–R762. https://doi.org/10.1016/j.cub.2021.04.001

[25] Jacquin, M. F., Chiaia, N. L., Haring, J. H., & Rhoades, R. W. (1990). Intersubnuclear connections within the rat trigeminal brainstem complex. Somatosensory & motor research, 7(4), 399-420.

[26] Jeong, M., Kim, Y., Kim, J., Ferrante, D. D., Mitra, P. P., Osten, P., & Kim, D. (2016). Comparative three-dimensional connectome map of motor cortical projections in the mouse brain. Scientific reports, 6(1), 1-14.

[27] DAVID KLEINFELD, RUNE W. BERG & SEAN M. O'CONNOR (1999) Invited Review Anatomical loops and their electrical dynamics in relation to whisking by rat, Somatosensory & Motor Research, 16:2, 69-88, DOI: 10.1080/08990229970528

[28] Lam, Y. W., & Sherman, S. M. (2007). Different topography of the reticulothalmic inputs to first-and higher-order somatosensory thalamic relays revealed using photostimulation. Journal of neurophysiology, 98(5), 2903-2909.

[29] Leão RN, Mikulovic S, Leão KE, Munguba H, Gezelius H, Enjin A, Patra K, Eriksson A, Loew LM, Tort AB, Kullander K. OLM interneurons differentially modulate CA3 and entorhinal inputs to hippocampal CA1 neurons.

Nat Neurosci. 2012 Nov;15(11):1524-30. doi: 10.1038/nn.3235. Epub 2012 Oct 7. PMID: 23042082; PMCID: PMC3483451.

[30] Lee, S., Carvell, G. E., & Simons, D. J. (2008). Motor modulation of afferent somatosensory circuits. Nature Neuroscience, 11(12), 1430–1438. https://doi.org/10.1038/nn.2227

[31] Lee, S. H., & Dan, Y. (2012). Neuromodulation of Brain States. Neuron, 76(1), 209–222. https://doi.org/10.1016/j.neuron.2012.09.012

[32] Liu, X., Huang, H., Snutch, T.P. et al. The Superior Colliculus: Cell Types, Connectivity, and Behavior. Neurosci. Bull. 38, 1519–1540 (2022). https://doi.org/10.1007/s12264-022-00858-1

[33] Ma, P. M. (1991). The barrelettes—architectonic vibrissal representations in the brainstem trigeminal complex of the mouse. Normal structural organization. Journal of Comparative Neurology, 309(2), 161-199.

[34] Madisen L, Zwingman TA, Sunkin SM, Oh SW, Zariwala HA, Gu H, Ng LL, Palmiter RD, Hawrylycz MJ, Jones AR, Lein ES, Zeng H. A robust and high-throughput Cre reporting and characterization system for the whole mouse brain. Nat Neurosci. 2010 Jan;13(1):133-40. doi: 10.1038/nn.2467. Epub 2009 Dec 20. PMID: 20023653; PMCID: PMC2840225.

[35] McElvain, L. E., Friedman, B., Karten, H. J., Svoboda, K., Wang, F., Deschênes, M., & Kleinfeld, D. (2018). Circuits in the Rodent Brainstem that Control Whisking in Concert with Other Orofacial Motor Actions. Neuroscience, 368, 152–170. https://doi.org/10.1016/j.neuroscience.2017.08.034

[36] Morrow JA, Collie IT, Dunbar DR, Walker GB, Shahid M, Hill DR. Molecular cloning and functional expression of the human glycine transporter GlyT2 and chromosomal localisation of the gene in the human genome. FEBS Lett. 1998 Nov 20;439(3):334-40. doi: 10.1016/s0014-5793(98)01390-8. PMID: 9845349.

[37] Muñoz-Castañeda, R., Zingg, B., Matho, K.S. et al. Cellular anatomy of the mouse primary motor cortex. Nature 598, 159–166 (2021). https://doi.org/10.1038/s41586-021-03970-w

[38] Nicolelis, M. A., Chapin, J. K., & Lin, R. C. (1992). Somatotopic maps within the zona incerta relay parallel GABAergic somatosensory pathways to the neocortex, superior colliculus, and brainstem. Brain research, 577(1), 134-141.

[39] Nicolelis, M., & Chapin, J. (1994). Spatiotemporal structure of somatosensory responses of many-neuron ensembles in the rat ventral posterior medial nucleus of the thalamus. The Journal of Neuroscience, 14(6), 3511–3532. https://doi.org/10.1523/jneurosci.14-06-03511.1994

[40] Oh, S. W., Harris, J. A., Ng, L., Winslow, B., Cain, N., Mihalas, S., ... & Zeng, H. (2014). A mesoscale connectome of the mouse brain. Nature, 508(7495), 207-214.

[41] Parolari, L. (2020). Dissection of Neurons and Circuits Involved in Regulating Innate Behaviors, Movement and Higher Cognitive Functions in Mice.

[42] Plummer, N. W., Chandler, D. J., Powell, J. A., Scappini, E., Waterhouse, B. D., & Jensen, P. (2020). An intersectional Viral-Genetic method for fluorescent tracing of axon collaterals reveals details of noradrenergic locus coeruleus structure. ENeuro, 7(3), ENEURO.0010-20.2020. https://doi.org/10.1523/eneuro.0010-20.2020

[43] Rang, H. P., Dale, M. M., Ritter, J. M., Flower, R. J., & Henderson, G. (2015). Rang and Dale's Pharmacology.

[44] Ruhl DA, Bomba-Warczak E, Watson ET, Bradberry MM, Peterson TA, Basu T, Frelka A, Evans CS, Briguglio JS, Basta T, Stowell MHB, Savas JN, Roopra A, Pearce RA, Piper RC, Chapman ER. Synaptotagmin 17 controls neurite outgrowth and synaptic physiology via distinct cellular pathways. Nat Commun. 2019 Aug 6;10(1):3532. doi: 10.1038/s41467-019-11459-4. PMID: 31387992; PMCID: PMC6684635.

[45] Safran M, Dalah I, Alexander J, Rosen N, Iny Stein T, Shmoish M, Nativ N, Bahir I, Doniger T, Krug H, Sirota-Madi A, Olender T, Golan Y, Stelzer G, Harel A, Lancet D. GeneCards Version 3: the human gene integrator. Database (Oxford). 2010 Aug 5;2010:baq020. doi: 10.1093/database/baq020. PMID: 20689021; PMCID: PMC2938269.

[46] Lee, E. Y., Hwang, Y. G., & Lee, H. S. (2017). Hypothalamic neuronal origin of neuropeptide Y (NPY) or cocaine- and amphetamine-regulated transcript (CART) fibers projecting to the tuberomammillary nucleus of the rat. Brain Research, 1657, 16-28. https://doi.org/10.1016/j.brainres.2016.11.025

[47] Shao-Ming Lu & Rick C.-S. Lin (1993) Thalamic Afferents of the Rat Barrel Cortex: A Light-and Electron-Microscopic Study Using Phaseolus vulgaris Leucoagglutinin as an Anterograde Tracer, Somatosensory & Motor Research, 10:1, 1-16, DOI: 10.3109/08990229309028819

[48] Smith, J. B., Watson, G. D., Alloway, K. D., Schwarz, C., & Chakrabarti, S. (2015). Corticofugal projection patterns of whisker sensorimotor cortex to the sensory trigeminal nuclei. Frontiers in Neural Circuits, 9, 160040. https://doi.org/10.3389/fncir.2015.00053

[49] Sokhadze, G., Campbell, P. W., & Guido, W. (2019). Postnatal development of cholinergic input to the thalamic reticular nucleus of the mouse. European Journal of Neuroscience, 49(8), 978-989.

[50] Stacey D, Bilbao A, Maroteaux M, Jia T, Easton AC, Longueville S, Nymberg C, Banaschewski T, Barker GJ, Büchel C, Carvalho F, Conrod PJ, Desrivières S, Fauth-Bühler M, Fernandez-Medarde A, Flor H, Gallinat J, Garavan H, Bokde AL, Heinz A, Ittermann B, Lathrop M, Lawrence C, Loth E, Lourdusamy A, Mann KF, Martinot JL, Nees F, Palkovits M, Paus T, Pausova Z, Rietschel M, Ruggeri B, Santos E, Smolka MN, Staehlin O, Jarvelin MR, Elliott P, Sommer WH, Mameli M, Müller CP, Spanagel R, Girault JA, Schumann G; IMAGEN Consortium. RASGRF2 regulates alcohol-induced reinforcement by influencing mesolimbic dopamine neuron activity and dopamine release. Proc Natl Acad Sci U S A. 2012 Dec 18;109(51):21128-33. doi: 10.1073/pnas.1211844110. Epub

2012 Dec 5. PMID: 23223532; PMCID: PMC3529066.

[51] Sumser, A., Mease, R. A., Sakmann, B., & Groh, A. (2017). Organization and somatotopy of corticothalamic projections from L5B in mouse barrel cortex. Proceedings of the National Academy of Sciences, 114(33), 8853-8858. https://doi.org/10.1073/pnas.1704302114

[52] Sun, P., Wang, J., Zhang, M., Duan, X., Wei, Y., Xu, F., ... & Zhang, Y. H. (2020). Sex-related differential whole-brain input atlas of locus coeruleus noradrenaline neurons. Frontiers in Neural Circuits, 14, 53.

[53] Takatoh, J., Park, J. H., Lu, J., Li, S., Thompson, P. M., Han, B. X., ... & Wang, F. (2021). Constructing an adult orofacial premotor atlas in Allen mouse CCF. Elife, 10.

[54] Taniguchi H, He M, Wu P, Kim S, Paik R, Sugino K, Kvitsiani D, Fu Y, Lu J, Lin Y, Miyoshi G, Shima Y, Fishell G, Nelson SB, Huang ZJ. A resource of Cre driver lines for genetic targeting of GABAergic neurons in cerebral cortex. Neuron. 2011 Sep 22;71(6):995-1013. doi: 10.1016/j.neuron.2011.07.026. Epub 2011 Sep 21. Erratum in: Neuron. 2011 Dec 22;72(6):1091. Kvitsani, Duda [corrected to Kvitsiani, Duda]. PMID: 21943598; PMCID: PMC3779648.

[55] Tasic B, Menon V, Nguyen TN, Kim TK, Jarsky T, Yao Z, Levi B, Gray LT, Sorensen SA, Dolbeare T, Bertagnolli D, Goldy J, Shapovalova N, Parry S, Lee C, Smith K, Bernard A, Madisen L, Sunkin SM, Hawrylycz M, Koch C, Zeng H. Adult mouse cortical cell taxonomy revealed by single cell transcriptomics. Nat Neurosci. 2016 Feb;19(2):335-46. doi: 10.1038/nn.4216. Epub 2016 Jan 4. PMID: 26727548; PMCID: PMC4985242.

[56] Tritsch NX, Oh WJ, Gu C, Sabatini BL. Midbrain dopamine neurons sustain inhibitory transmission using plasma membrane uptake of GABA, not synthesis. Elife. 2014 Apr 24;3:e01936. doi: 10.7554/eLife.01936. PMID: 24843012; PMCID: PMC4001323.

[57] Uhlén M, Fagerberg L, Hallström BM, Lindskog C, Oksvold P, Mardinoglu A, Sivertsson Å, Kampf C, Sjöstedt E, Asplund A, Olsson I, Edlund K, Lundberg E, Navani S, Szigyarto CA, Odeberg J, Djureinovic D, Takanen JO, Hober S, Alm T, Edqvist PH, Berling H, Tegel H, Mulder J, Rockberg J, Nilsson P, Schwenk JM, Hamsten M, von Feilitzen K, Forsberg M, Persson L, Johansson F, Zwahlen M, von Heijne G, Nielsen J, Pontén F. Proteomics. Tissue-based map of the human proteome. Science. 2015 Jan 23;347(6220):1260419. doi: 10.1126/science.1260419. PMID: 25613900.

[58] Venkataraman, A., Hunter, S. C., Dhinojwala, M., Ghebrezadik, D., Guo, J., Inoue, K., Young, L. J., & Dias, B. G. (2021). Incerto-thalamic modulation of fear via GABA and dopamine. Neuropsychopharmacology, 46(9), 1658-1668. https://doi.org/10.1038/s41386-021-01006-5

[59] Voigts, J., Sakmann, B., & Celikel, T. (2008). Unsupervised Whisker Tracking in Unrestrained Behaving Animals. Journal of Neurophysiology, 100(1), 504–515. https://doi.org/10.1152/jn.00012.2008

[60] Voigts, J., Herman, D., & Celikel, T. (2015). Tactile object localization by

anticipatory whisker motion. Journal of Neurophysiology, 113(2), 620–632. https://doi.org/10.1152/jn.00241.2014

[61] Volta M, Viaro R, Trapella C, Marti M, Morari M. Dopamine-nociceptin/orphanin FQ interactions in the substantia nigra reticulata of hemiparkinsonian rats: involvement of D2/D3 receptors and impact on nigro-thalamic neurons and motor activity. Exp Neurol. 2011 Mar;228(1):126-37. doi: 10.1016/j.expneurol.2010.12.024. Epub 2011 Jan 6. PMID: 21215744.

[62] Vitrac, C., & Benoît-Marand, M. (2017). Monoaminergic modulation of motor cortex function. Frontiers in Neural Circuits, 11. https://doi.org/10.3389/fncir.2017.00072

[63] Wang, J., Wang, X., Xia, M., Liao, X., Evans, A., & He, Y. (2015). GRETNA: a graph theoretical network analysis toolbox for imaging connectomics. Frontiers in human neuroscience, 9, 386.

[64] Wang, Q., Ding, S. L., Li, Y., Royall, J., Feng, D., Lesnar, P., Graddis, N., Naeemi, M., Facer, B., Ho, A., Dolbeare, T., Blanchard, B., Dee, N., Wakeman, W., Hirokawa, K. E., Szafer, A., Sunkin, S. M., Oh, S. W., Bernard, A., . . . Ng, L. (2020). The Allen Mouse Brain Common Coordinate Framework: A 3D Reference Atlas. Cell, 181(4), 936–953.e20. https://doi.org/10.1016/j.cell.2020.04.007

[65] Watts, D. J., & Strogatz, S. H. (1998). Collective dynamics of 'small-world'networks. nature, 393(6684), 440-442.

[66] Woolsey, T. A., & Van der Loos, H. (1970). The structural organization of layer IV in the somatosensory region (SI) of mouse cerebral cortex: the description of a cortical field composed of discrete cytoarchitectonic units. Brain research, 17(2), 205-242.

[67] Yang, Y., Jiang, T., Jia, X., Yuan, J., Li, X., & Gong, H. (2022). Whole-Brain Connectome of GABAergic Neurons in the Mouse Zona Incerta. Neuroscience Bulletin, 1-15.

[68] Zakiewicz, I. M., Bjaalie, J. G., & Leergaard, T. B. (2014). Brain-wide map of efferent projections from rat barrel cortex. Frontiers in Neuroinformatics, 8. https://doi.org/10.3389/fninf.2014.00005

[69] Zeisel A, Hochgerner H, Lönnerberg P, Johnsson A, Memic F, van der Zwan J, Häring M, Braun E, Borm LE, La Manno G, Codeluppi S, Furlan A, Lee K, Skene N, Harris KD, Hjerling-Leffler J, Arenas E, Ernfors P, Marklund U, Linnarsson S. Molecular Architecture of the Mouse Nervous System. Cell. 2018 Aug 9;174(4):999-1014.e22. doi: 10.1016/j.cell.2018.06.021. PMID: 30096314; PMCID: PMC6086934.

[70] Zhou, M., Liu, Z., Melin, M.D. et al. A central amygdala to zona incerta projection is required for acquisition and remote recall of conditioned fear memory. Nat Neurosci 21, 1515–1519 (2018). https://doi.org/10.1038/s41593-018-0248-4

Supplementary Materials

TG line	Classification	Source
A930038C07Rik-Tg1-Cre	Excitatory	Harris et al., 2014
Adycap1-2A-Cre	Uncategorized	Zeisel et al., 2018
Calb2-IRES-Cre	Inhibitory	Taniguchi et al., 2011
Calb1-T2A-dgCre	Inhibitory	Daigle et al., 2018
Cart-IRES2-Cre	Uncategorized	Zeisel et al., 2018
Cart-Tg1-Cre	Uncategorized	Zeisel et al., 2018
Cck-IRES-Cre	Uncategorized	Taniguchi et al., 2011
Chat-IRES-Cre-neo	Uncategorized	Zeisel et al., 2018
Chrna2-Cre-OE25	Inhibitory	Leão et al., 2012
Cort-T2A-Cre	Inhibitory	Taniguchi et al., 2011
ctgf-T2A-dgCr	Excitatory	Tasic et al., 2016
Cux2-CreERT2	Excitatory	Zeisel et al., 2018
Drd3-Cre-KI196	Inhibitory	Volta et al., 2011
Efr3a-Cre-NO108	Uncategorized	Zeisel et al., 2018
Erbb4-T2A-CreERT2	Inhibitory	Madisen et al., 2010
Gabrr3-Cre-KC112	Inhibitory	Parolari 2020
Gad2-IRES-Cre	Inhibitory	Taniguchi et al., 2011
Gal-Cre-KI87	Excitatory	Zeisel et al., 2018
Grik4-Cre	Uncategorized	Zeisel et al., 2018
Htr2a-Cre-KM20	Excitatory	Rang et al., 2015
Lypd6-Cre-KL156	Uncategorized	Zeisel et al., 2018
Nos1-CreErt2	Inhibitory	Taniguchi et al., 2011
Npr3-IRES2-Cre	Excitatory	Daigle et al., 2018
Ntrk1-IRES-Cre	Uncategorized	Zeisel et al., 2018
Ntsr1-Cre-GN220	Excitatory	Madisen et al., 2010
Oxtr-Cre-ON66	Uncategorized	Zeisel et al., 2018
Oxtr-T2A-Cre	Uncategorized	
Pdzk1ip1-Cre-KD31	Uncategorized	Van der Togt et al., 1991
Plxnd-Cre-OG	Excitatory	Zeisel et al., 2018
Ppp1r17-Cre-NL1	Inhibitory	Zeisel et al., 2018
Prkcd-GluCla-CFP-IRES	Uncategorized	Zeisel et al., 2018
Pvalb-IRES-Cre	Inhibitory	Madisen et al., 2010
Rasgrf2-T2A-dCre	Uncategorized	Stacey et al., 2012
Rbp4-Cre-Kl100	Excitattory	Zeisel et al., 2018
Rorb-IRES-Cre	Uncategorized	Zeisel et al., 2018
Scnn1a-Tg3-Cre	Excitatory	Madisen et al., 2010
Sepw1-Cre-NP39	Uncategorized	Zeisel et al., 2018
Sim1-Cre-KJ18	Excitatory	Zeisel et al., 2018
Slc6a3-Cre	Uncategorized	Zeisel et al., 2018
Slc6a4-Cre-ET33	Uncategorized	Zeisel et al., 2018
Slc6a4-CreERT2-EZ13	Uncategorized	Zeisel et al., 2018
Slc6a5-Cre-KF10	Inhibitory	Morrow et al., 1998
Slc17a6-IRES-Cre	Excitatory	Harris et al., 2014
Slc17a8-IRES2-Cre	Excitatory	Tasic et al., 2018

Slc18a2-Cre-OZ14	Excitatory	Tritsch et al., 2014
Slc32a1-IRES-Cre	Inhibitory	Harris et al., 2014
Sst-IRES-Cre	Inhibitory	Taniguchi et al., 2011
Syt6-Cre-KI148	Uncategorized	Safran et al., 2010
Syt17-Cre-NO14	Excitatory	Ruhl et al., 2019
Tlx3-Cre-PL56	Excitatory	Cheng et al. 2004
Th-Cre-FI172	Uncategorized	Uhlèn et al., 2015

Supplemental Table 1 - Type of neuron marked by each transgenic line

structure	wild type experiments	transgenic line experiments	transgenic lines	expressed in number of structures	transgenic line showing connections
MOp	8	21	15	13	12
ZI	4	15	13	11	11
PO	3	6	3	3	3
bfd	6	40	29	21	16
PSV	2	1	2	1	1
VTA	2	12	12	9	8
SI	7	10	8	7	7
SPVO	1	0	0	0	0
LC	0	0	0	0	0
SC	7	14	9	7	7
TM	0	1	1	0	0
VPM	3	6	6	5	5
VII	2	5	4	3	3
PPN	0	3	3	2	2
SPVC	3	6	6	5	5
SPVI	2	2	1	1	1
RT	2	11	7	7	7
DR	0	9	5	4	4

Supplemental Table 2 - For each structure, this table presents the number of experiments ran (transgenic and wild), the number of transgenic lines tested, the number of transgenic lines showing marked neurons in the considered structures and the number of transgenic lines showing a connection.

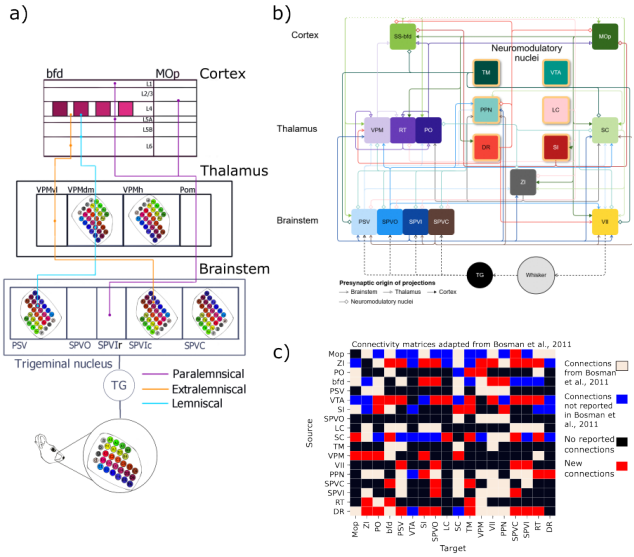

Supplemental Fig. 1 a) The whisker pad is organized in a grid-like structure. Each whisker is represented in SPVI, PSV, VPM, and bfd by an agglomerate of neurons organized in a barrel-like shape, respecting the coordinates of the whisker on the whisker pad with rotations. The information from the whisker enters the system through the trigeminal ganglion, projecting to the trigeminal nuclei. Here the information flow is divided into three major pathways: 1) the lemniscal pathway (blue), originating from the barrelettes of PSV, ascending to the barreloids of VPMdm and ending in the barrels of the layer 4 of the somatosensory pathway; 2) the extralemniscal pathway (orange), taking its origin in interbarrelette neurons of SPVI, connecting to VPMvl and targeting the primary somatosensory cortex; and 3) the paralemniscal pathway (purple), taking its source in SPVI, targeting PO, which then targets MOp and bfd. b) The connectivity map presented by Bosman et al. (2011). It describes 72 connections across the 18 considered nuclei. c) The summary of the connections identified by Bosman and colleagues (color code: creme), experimentally identified connections since 2011 (blue), newly discovered anatomical projections identified in this work (red), and no known connections (black).

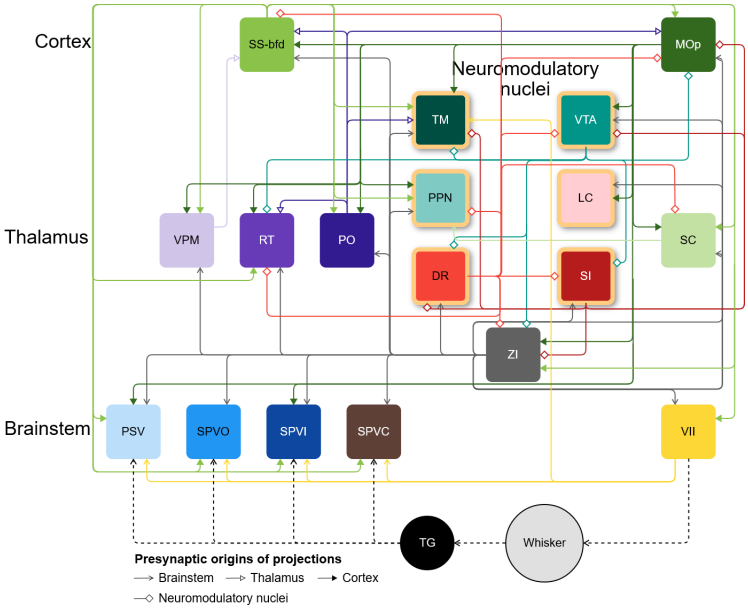

Supplemental Fig. 2 The excitatory connectivity map contains 73 connections.

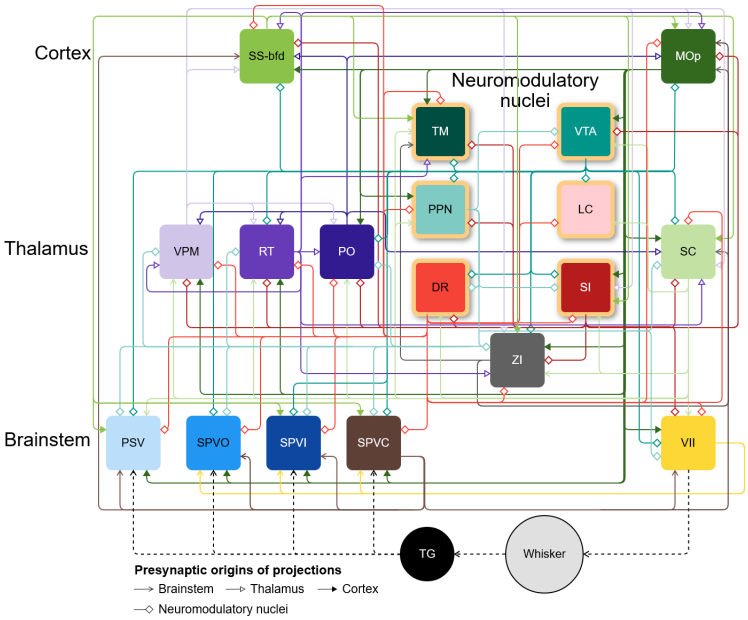

Supplemental Fig. 3 124 connections were revealed by uncategorized transgenic lines.

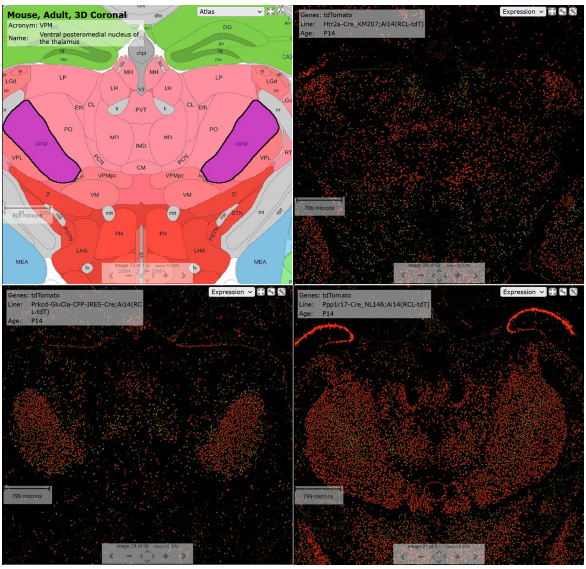

Supplemental Fig. 4 Expression in VPM of the transgenic lines PPP1r17 (inhibitory), Htr2a (Excitatory), and Prkcd (Uncategorized)